ACS APPLIED MATERIALS & INTERFACES

Research Article

www.acsami.org

Mesoporous Phosphorus-Doped g-C_3N_4 Nanostructured Flowers with Superior Photocatalytic Hydrogen Evolution Performance

Yun-Pei Zhu,[†] Tie-Zhen Ren,[‡] and Zhong-Yong Yuan*[,†]

[†]Key Laboratory of Advanced Energy Materials Chemistry (Ministry of Education), Collaborative Innovation Center of Chemical Science and Engineering (Tianjin), College of Chemistry, Nankai University, Tianjin 300071, China

[‡]School of Chemical Engineering and Technology, Hebei University of Technology, Tianjin 300130, China

Supporting Information

ABSTRACT: Graphitic carbon nitride (g-C_3N_4) has been deemed a promising heterogeneous metal-free catalyst for a wide range of applications, such as solar energy utilization toward water splitting, and its photocatalytic performance is reasonably adjustable through tailoring its texture and its electronic and optical properties. Here phosphorus-doped graphitic carbon nitride nanostructured flowers of in-plane mesopores are synthesized by a co-condensation method in the absence of any templates. The interesting structures, together with the phosphorus doping, can promote light trapping, mass transfer, and charge separation, enabling it to perform as a more impressive catalyst than its pristine carbon nitride counterpart for catalytic hydrogen evolution under visible light irradiation. The catalyst has low cost, is environmentally friendly, and represents a potential candidate in photoelectrochemistry.

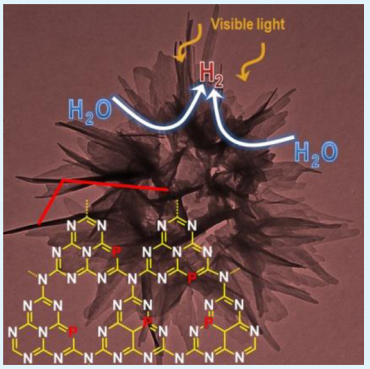

KEYWORDS: *graphitic carbon nitride, phosphors doping, mesoporosity, nanostructures, photocatalysis, hydrogen evolution*

1. INTRODUCTION

Currently, with the rapid consumption of conventional fossil energy, a pivotal goal of modern chemistry is to imitate the natural photosynthesis systems to create energy storage host materials. In this context, semiconductor-mediated harvest and conversion of solar energy through water photolysis to produce clean hydrogen energy is considered as a sustainable and prospective solution to alleviate the energy crisis and environmental issues.[1,2] The central difficulty of the field lies in the pursuit of sustainable and efficient candidates of basic working principles that take full advantage of visible light. To date, a variety of earth-abundant semiconductor photocatalysts such as metal oxides, sulfides, and selenides have been explored in an attempt to realize photocatalytic water splitting,[3−6] though the classical photocatalytic systems are prohibited by the insufficient light absorbance and limited charge transfer capability. Developing new materials with appropriate bandgaps and catalytic functions is considerably imminent. As known for plastic optoelectronics, supermolecule- or polymer-based systems have been attempted to initiate hydrogen evolution, but with ultraviolet light only and rapid deconstruction under excitation.[7,8] Alternatively, graphitic carbon nitride (g-C_3N_4), a kind of polymeric semiconductor that possesses a graphite-like layered structure, has been exemplified as a metal-free candidate for solar energy conversion, due to the controllable bandgaps, suitable band positions, tailorable textures, and high stability.[9−14] Of particular interest is that this two-dimensional conjugated semiconductor could catalyze solar water splitting and organic photosynthesis even without the optimization of textual and electronic properties,[15−17] but there is still much room to improve the catalytic efficiency.

As compared with the bulk counterparts, nanostructures with specific morphologies can not only contribute to accelerate the separation and movement of photoinduced charge carriers at the materials interface but also facilitate mass transfer and provide sufficient active sites for reaction. Highly anisotropic g-C_3N_4 nanosheets prepared via thermal oxidation etching of bulk sample in air promise the superior catalytic activity for hydrogen evolution under visible light irradiation than the bulk counterpart.[18] Thermal polycondensation of molecular cooperative assembly derived melamine cyanuric acid complex would lead to mesoporous g-C_3N_4 hollow spheres that demonstrated increased lifetime of photoexicited charge carriers,[19] while silica spheres could perform as sacrificial scaffolds to construct spherical carbon nitride frameworks.[20,21] Besides, other diverse types of g-C_3N_4 nanostructures including mesostructures, nanorods, nanotubes, and nanofibers with enhanced performance have been achieved,[22−25] suggesting that structural engineering paves a promising way to rationally design and optimize the g-C_3N_4 photocatalyst. Noticeably, the general synthesis involves preformed functionalized templates and complicated removal procedures, which is unfavorable from the viewpoint of practical application and may cause damage to the nanostructures. On the other hand, it is noteworthy that the

Received: June 7, 2015
Accepted: July 17, 2015
Published: July 17, 2015

DOI: 10.1021/acsami.5b04947
ACS Appl. Mater. Interfaces 2015, 7, 16850−16856

polymeric nature of g-C_3N_4 makes the ample choice of chemical protocols possible to introduce foreign atoms into the graphitized backbone so as to alter the optical and electronic properties.[26,27] For instance, doping g-C_3N_4 with heteroatoms, such as B, S, P, and I,[28−31] is expected to present a homogeneous functionalization through the bulk matrixes and extended electronic possibilities. Nevertheless, it remains a challenge to simultaneously achieve the nanostructuring and doping of g-C_3N_4 through a facile and cost-effective strategy.

In this work, to exhibit the above considerations, flower-like P-doped g-C_3N_4 (P-CN) nanostructure is synthesized by a template-free phosphonic-mediated route, wherein P can affect the polycondensation process and conformation of the resulting g-C_3N_4, thereby offering a direction role to modify the texture and electronic structures. The remarkable electronic structural properties were evidenced by a series of spectroscopy and electrochemical analyses, suggesting the great potency in photocatalytic H_2 evolution under visible light illumination, largely outperforming the bulk pristine g-C_3N_4 counterpart.

2. EXPERIMENTAL SECTION

2.1. Synthesis of Phosphorus-Doped g-C_3N_4 (P-CN). Melamine and (hydroxyethylidene)diphosphonic acid (HEDP) with a mass ratio of 12:1 were dissolved in the mixed solution of deionized distilled water and ethylene glycol with a volume ratio of 15:1, followed by evaporation under constant heating and magnetic stirring. Then, the white samples were further dried at 60 °C under vacuum conditions overnight. The resulting mixture was heated in a quartz container from room temperature to 500 °C and stabilized for 3 h in N_2 flow. The ultimate dark brown materials were named as P-CN.

2.2. Preparation of Pure Bulk g-C_3N_4. For comparison purpose, the same procedure as that used for the preparation of P-CN was performed, except that HEDP was not added to the synthesis system.

2.3. Fabrication of Mesoporous g-C_3N_4. In a typical synthesis procedure, melamine was dissolved in a dispersion of SiO_2 nanoparticles of 15 nm in water with gentle stirring at 85 °C for about 3 h to evaporate the water. Then, the resulting white powder was heated at a rate of 2.5 °C min^{-1} over 4 h to 500 °C and stabilized for an additional 3 h. The resulting brown-yellow powder was stirred in 200 mL of 1 M HF for 12 h, followed by filtration and washing with 150 mL of H_2O and 100 mL of ethanol. The procedure was repeated three times to guarantee the complete removal of silica template. Finally, the resultant powders were dried at 100 °C overnight. The ultimate product was mesoporous g-C_3N_4.

2.4. Synthesis of g-C_3N_4 Nanosheets. Bulk g-C_3N_4 was prepared by heating melamine from the room temperature to 500 °C with a ramp rate of 2.5 °C min^{-1} in inert protective gas, and then the temperature was kept at 500 °C for 4 h. Then, 50 mg of the yellow solids was dispersed in 100 mL of a mixed solution of water and isopropyl alcohol (1:10), followed by sonication for about 10 h. The mixture was centrifuged at 2800 rpm to remove unexfoliated aggregates, leaving a homogeneous aqueous dispersion of g-C_3N_4 nanosheets. Finally, the light-yellow exfoliated g-C_3N_4 nanosheets were obtained.

2.5. Physicochemical Characterization. Transmission electron microscopy (TEM) was carried out on a Jeol JEM-2100F at 200 kV. X-ray diffraction (XRD) patterns were recorded on a Bruker D8 Focus diffractometer with Cu Kα radiation (λ = 1.5418 Å) operated at 40 kV and 40 mA. N_2 adsorption−desorption isotherms were measured on a Quantachrome Autosorb-1 sorption analyzer at liquid nitrogen temperature (77 K). The samples were degassed at 200 °C overnight prior to the measurements. The specific surface area was determined by the Brunauer−Emmett−Teller (BET) method using the adsorption data in the relative pressure range of P/P_0 = 0.05−0.3. Thermogravimetry analysis (TGA) was performed on a TA SDT Q600 instrument at a heating rate of 10 °C min^{-1} in the air atmosphere with α-Al_2O_3 as the reference. Diffuse reflectance UV−vis absorption spectroscopy was performed with a Shimadzu UV-2450 spectrophotometer, with $BaSO_4$ performing as a reference. Photoluminescence (PL) spectra were measured at ambient temperature on a Hitachi F-4500 FL fluorescence spectrophotometer. X-ray photoelectron spectroscopy (XPS) measurements were performed with a Kratos Axis Ultra DLD (delay line detector) spectrometer equipped with a monochromatic Al Kα X-ray source (1486.6 eV). All XPS spectra were recorded by using an aperture slot of 300 × 700 μm; survey spectra were recorded with a pass energy of 160 eV and high-resolution spectra with a pass energy of 40 eV.

2.6. Electrochemical Measurements. Electrochemical tests were carried out on a Zennium (Zahner, Germany) workstation in a three-electrode model, utilizing a Pt wire as the counter electrode and an Ag/AgCl electrode as the reference electrode. Typically, for the preparation of working electrodes, 50 mg of the photocatalyst powder was mixed with a trace mount of distilled water and ethanol and an aliquot amount of poly(ethylene glycol) and emulsifier, followed by blending in a mortar to get a homogeneous mixture. The slurry was then spread onto a 1.5 × 2 cm fluorine-doped tin oxide (FTO) glass electrode. Electrodes were calcined in air at 400 °C for 1 h to eliminate the organic additives completely. The electrochemical impedance spectroscopy (EIS) frequency ranged from 10 m to 100 kHz in parallel with the alternating current signal amplitude of 10 mV. The polarization curves were conducted in the same above-mentioned three-electrode system, while the bias sweep range was from −0.9 to −1.5 V vs Ag/AgCl with a step size of 5 mV.

2.7. Photocatalytic Activity for Water Splitting. Photocatalytic water splitting (H_2 evolution) experiments with the use of triethanolamine as sacrificial agent were carried in a Pyrex top-irradiation reaction vessel connected to a glass closed gas system. H_2 production was conducted via dispersing 50 mg of catalyst powder in an aqueous solution (100 mL) containing 10 wt % triethanolamine in the reaction cell, while 3 wt % Pt was photodeposited from H_2PtCl_6 aqueous solution as cocatalyst, resulting a near neutral condition in the reaction system. Before irradiation, the system was bubbled with Ar for 30 min to remove air and ensure anaerobic conditions in the reaction system, followed by the visible light irradiation with a 300W Xenon arc lamp (Shenzhen Shengkang Technology Co., Ltd.). The wavelength of the incident light was controlled by applying some appropriate long-pass cutoff filters, and the aqueous temperature was maintained around room temperature by a flow of cooling water during the photocatalytic reaction. The evolved gases were analyzed by gas chromatography equipped with a thermal conductive detector (TCD) and a 5 Å molecular sieve column, using Argon as the carrier gas.

3. RESULTS AND DISCUSSION

Typically, the precursors of g-C_3N_4 (melamine) and P source (organophosphonic acid) were homogeneously mixed first in a one-pot fashion, allowing the acid−base interaction between melamine and phosphonic groups to facilitate the cross-linking. A further treatment at 500 °C in the atmosphere of nitrogen gas then resulted in the decomposition and polymerization to finally yield P-doped g-C_3N_4 (abbreviated as P-CN), while the high thermal stability of phosphonic source (over 500 °C; Figure S1, Supporting Information) ensures the substantial and homogeneous P doping. P-CN still retains high stability around 500 °C, almost equal to that of bulk g-C_3N_4 that synthesized in the absence of organophosphonic source.

Micromorphological analysis by TEM reveals that pristine g-C_3N_4 sample is of layered platelet-like surface morphology (Figure 1a and Figure S2). Distinctively, P-CN is assembled from nanosheets that directed from the center and interconnected together as nanostructured flowers (Figure 1b and Figure S3). Deep magnification shows that in-plane mesopores of several to tens of nanometers are randomly distributed on the carbon nitride nanosheets (Figure 1c). The peculiar nanostructures endows P-CN with open-up surface

DOI: 10.1021/acsami.5b04947
ACS Appl. Mater. Interfaces 2015, 7, 16850−16856

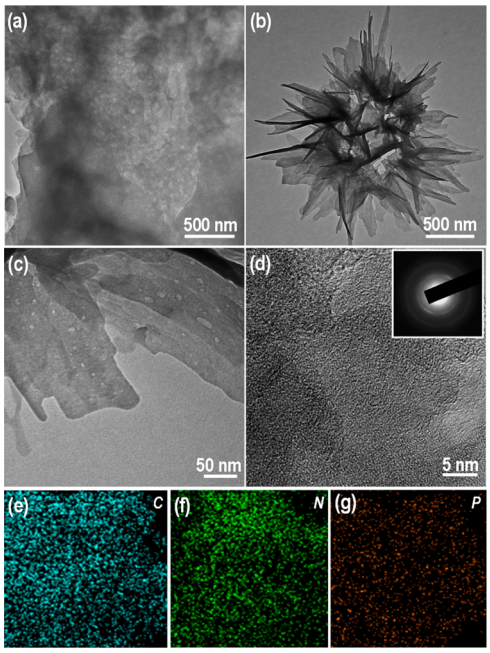

Figure 1. TEM images of (a) g-C_3N_4 and (b–d) P-CN. (d, inset) SAED pattern. (e–g) EDS elemental mapping images of P-CN.

and well-defined mesopores, which can provide enriched active sites and simultaneously promote mass transfer and charge separation in nanodomains, thus optimizing the π-conjugated system for photochemical applications.[23,32,33] High-resolution TEM image in Figure 1d manifests the multicrystalline nature of P-CN, consistent with the polycrystalline diffraction rings in the selected area electron diffraction (SAED) pattern (inset of Figure 1d), indicating that P-CN consists of stacked graphitic planes constructed from the triazine building units. Energy dispersive X-ray spectroscopy (EDS) elemental mapping images verify the uniform distribution of C, N, and P throughout P-CN at the nanoscale.

The textual information on the synthesized g-C_3N_4 samples was accessed by nitrogen sorption measurement (Figure 2). The adsorption isotherm for P-CN is between type II and IV together with an obvious capillary condensation step, characteristics of mesoporous materials according to the IUPAC classification.[34,35] The pore size distribution based on nonlocal density functional theory (NLDFT) method exhibits the

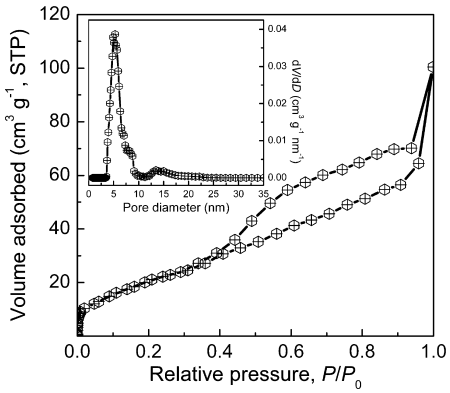

Figure 2. N_2 adsorption–desorption isotherm of P-CN and (inset) the corresponding pore size distribution curve on the basis of NLDFT method.

existence of mesopores from 3 to 18 nm, which is in good agreement with TEM analysis. Note that evident adsorption isotherm of type III for g-C_3N_4 indicates the inferior architectural property in comparison with P-CN. The specific surface area calculated from the linear part of the multipoint plot of P-CN is 83 m^2 g^{-1}, much higher than that of g-C_3N_4 (7 m^2 g^{-1}; Figure S4). Indeed, the involvement of heteroatom moieties (i.e., diphosphonic acid) could strongly interact with melamine on the basis of acid–base cross-linking effect and thus in situ turn the polymerization way during the high-temperature calcination process;[36,37] and the incorporation of P atoms (larger than C and N atoms) as doping and leaving motifs could disturb the structure of graphitic g-C_3N_4, akin to the heteroatom-assisted "bottom-up" synthesis of g-C_3N_4 nanosheets.[37] The delamination effect induced by doping could benefit the condensation of carbon nitride layers in the nanodomains to lessen the surface tension,[22,36–38] leading to the formation of P-doped g-C_3N_4 nanoflowers possibly due to the self-assembly effect resulted from the altered pyrolysis processes. On the other hand, the difference of dissolution ability of organophosphonic acid in water and alcohol (ethylene glycol used herein) would favor the formation of microemulsion, which performed as templates for mesopores during the calcination procedure (Figure S5).

The crystalline structure of g-C_3N_4 is well preserved in the P-CN material, as confirmed by two feature signals on the XRD pattern (Figure 3a) that show a main contribution around 2θ = 27.3° related to the (100) peak for the in-plane structural packing motif along with a shoulder diffraction situated at 2θ = 13.1° attributed to the (002) peak for in-planar repeated tri-*s*-triazine units.[21–24,39,40] Additionally, the additional weak diffractions situated at about 17.6 and 22.2° can be attributed to (600) and (650) planes of graphitic carbon nitride, respectively, which results from the denser packing or a distortion of the melon structure in which every second melon sheet is displaced.[41] Notably, the overall weakened intensity is examined for P-CN, indicating that doping P into the g-C_3N_4 network can significantly reduce the correlation length of interlayer periodicity and particle size, correlating well with the TEM observation.

The molecular structure information on the carbon nitride materials was illustrated by FT–IR spectra, as depicted in Figure 3b. With respect to g-C_3N_4, the prominent bands in the region of 1200–1650 cm^{-1} can be related to the typical stretching modes of CN heterocycles, wherein the peaks at 1241, 1318, and 1425 cm^{-1} are assigned to the aromatic C–N stretching.[9,10] The sharp band at 805 cm^{-1} is attributed to the out-of-plane bending vibration of characteristics of triazine rings. The broad peaks at around 2900–3400 cm^{-1} originate from stretching vibration modes for the –NH and hydroxyl of the adsorbed H_2O. The FT–IR spectrum of P-CN resembles g-C_3N_4 in the characteristic bands, which signifies that the typical graphitic structure of carbon nitride was well maintained even after chemical doping of P heteroatom. The vibration band corresponding to P-related functional groups can hardly be observed, except for a weak peak located at about 950 cm^{-1} that is assigned to P–N stretching mode,[30,42] which is presumably owing to the overlap of the bands with those of strong C–N vibrations.

Moreover, XPS were conducted to investigate the chemical environment and surface stoichiometry. The XPS survey spectrum in Figure 3c shows that the P-CN sample contains only C, N, P and O species without other impurities. The XPS

DOI: 10.1021/acsami.5b04947
ACS Appl. Mater. Interfaces 2015, 7, 16850–16856

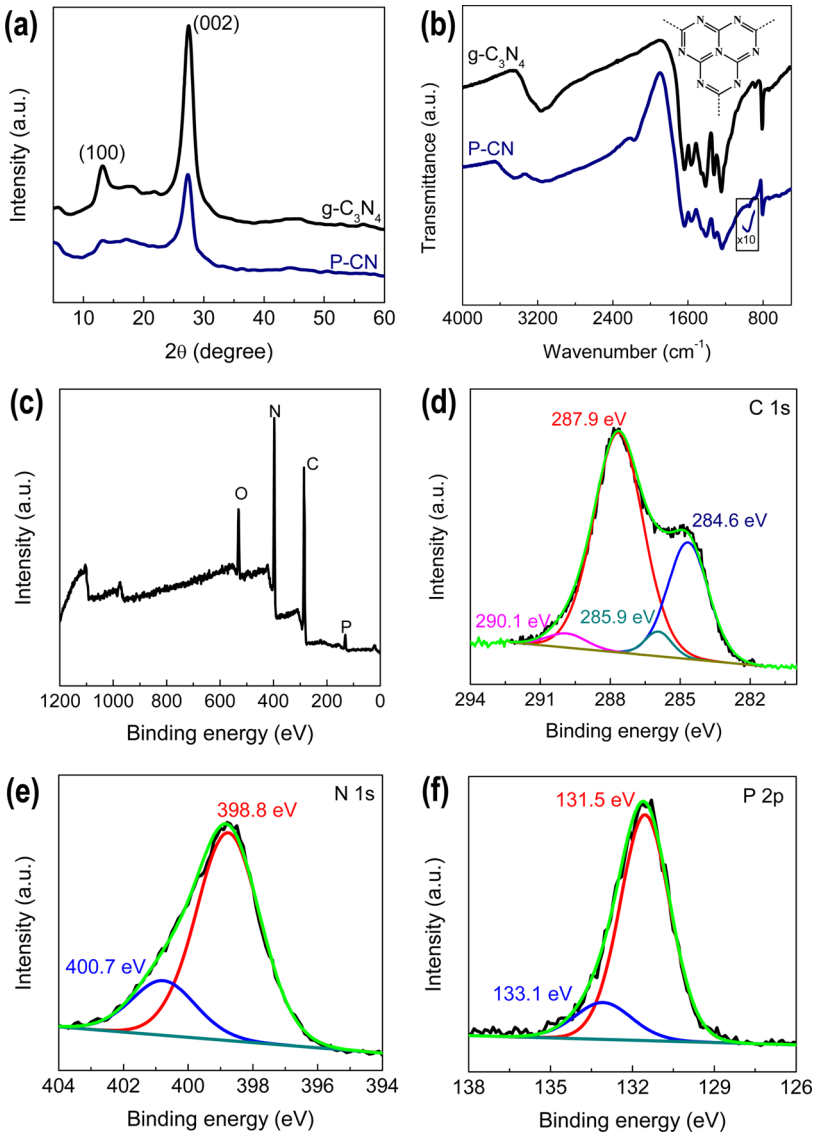

Figure 3. (a) XRD patterns and (b) FT-IR spectrum of g-C_3N_4 and P-CN. (c) XPS survey spectrum and high-resolution XPS spectra of (d) C 1s, (e) N 1s, and (f) P 2p core levels in P-CN.

spectra of the C 1s core level for P-CN can be deconvoluted into four components including the standard reference carbon (284.6 eV), C−N (285.9 eV), and the sp^2-bonded C in N═C(−N)$_2$ (287.9 eV), while the peak at 290.1 eV sp^2-hybridized carbon in the aromatic ring attached to the NH_2 group,[10] resulting from the incomplete condensation of melamine during the high-temperature heat treatment (Figure 3d). High-resolution N 1s spectrum in Figure 3e can be fitted into two components. The dominant peak at 398.8 eV refers to aromatic N in triazine rings (C═N−C), and a weak shoulder at high binding energy of 400.7 eV is attributable to the sp^2-hybridized N bonded to three atoms (C−N(−C)−C or C−N(H)−C).[19,20,43,44] Also, the P 2p spectrum can be fitted into two components (Figure 3f). The sharp peak centered at 131.5 eV is assigned to P−C and the weak one at 133.1 eV is typical for P−N coordination,[30,42−44] indicating that P most probably substitutes C or N in g-C_3N_4 framework to form P−N or P−C bonds, whereas that of bulky g-C_3N_4 naturally shows no detectable contributions (Figure S6). P content is determined to be 1.3 atom % on the basis of XPS analysis for P-CN, and the corresponding C/N atomic ratio is 0.67, which is close to the theoretical value of graphitic carbon nitride (0.75).

The introduction of P atoms into the g-C_3N_4 polymeric skeleton alters the structural and electronic aspects and thus the resultant optical/electronic properties. This influence can be reflected by the color change from pale yellow for undoped g-C_3N_4 to dark brown after P doping (Figure 4a inset), which can further be quantified by the optical absorption spectra (Figure 4a). Pure g-C_3N_4 displays typical semiconductor absorption of graphitic carbon nitride at the blue region, together with a bandgap of about 2.70 eV. In contrast, it is found that the optical absorption band edge for P-CN is shifted to lower bandgap energies, implying a bandgap narrowing and the electronic integration of P atoms in the lattice of g-C_3N_4 as well. This modification accompanied by the unique nanostructures, in principle, can improve the capability to harvest visible light and favor the mass transfer and charge transport, creating a platform in efficient heterogeneous photocatalysis.

The synthesized g-C_3N_4 semiconductors are therefore evaluated in an assay of H_2 production from water under visible light irradiation using triethanolamine as sacrificial agent.

DOI: 10.1021/acsami.5b04947
ACS Appl. Mater. Interfaces 2015, 7, 16850−16856

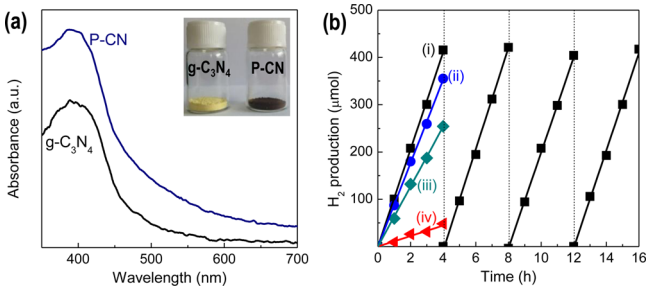

Figure 4. (a) UV−vis diffuse reflectance spectra of g-C_3N_4 and P-CN and (inset) photographs of (left) g-C_3N_4 and (right) P-CN. (b) Photocatalytic water reduction with the use of the synthesized graphitic carbon nitride materials under visible light illumination: (i) P-CN, (ii) g-C_3N_4 nanosheet, (iii) mesoporous g-C_3N_4, and (iv) g-C_3N_4.

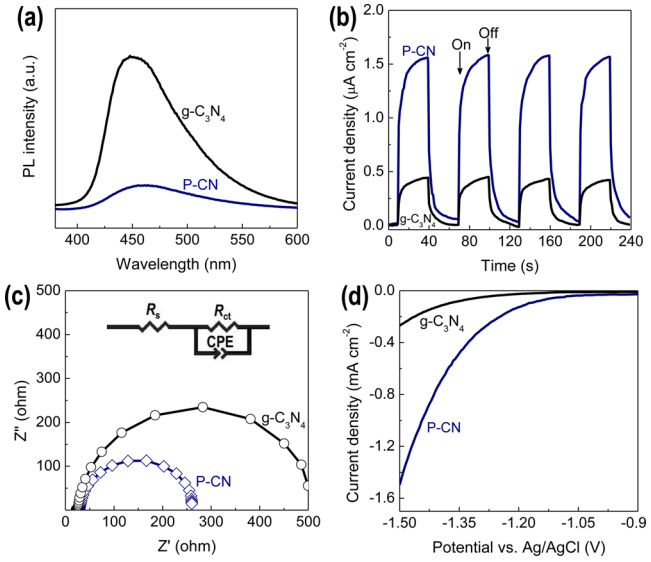

Figure 5. (a) Photoluminescence spectra, (b) photocurrent response, (c) EIS Nyquist plots, and (d) polarization curves of P-CN and g-C_3N_4.

As shown in Figure 4b, a remarkably enhanced H_2 evolution rate of 104.1 μmol h^{-1} is achieved on P-CN, tremendously exceeding that of pure g-C_3N_4 reference (11.2 μmol h^{-1}). The corresponding activity virtually outperforms a number of inorganic semiconductor photocatalysts. In order to present the superiority of P-CN, two additional g-C_3N_4 samples, mesoporous g-C_3N_4 and g-C_3N_4 nanosheets, were investigated under the identical conditions (Figure 4b). Although these two g-C_3N_4 samples are of higher specific surface areas (216 m^2 g^{-1} for mesoporous g-C_3N_4 and 273 m^2 g^{-1} for g-C_3N_4 nanosheet), the catalytic activities are inferior compared with P-CN, which indicates that the synergic effect of nanostructures and P doping is able to attain increased surface reactivity for the photocatalytic reaction (Figure S7). Durability is another crucial criterion for practical application. As such, the catalytic stability of P-CN was evaluated under a prolonged visible light illumination duration of 16 h. No obvious attenuation of photocatalytic H_2 evolution rate for P-CN can be seen after 4 consecutive cycling tests, meaning the good stability against photocorrosion. The recovered catalyst powders show no obvious alternation in the XRD patterns, FT-IR spectrum and micromorphology (Figure S8), which suggests the robust nature of the heteroatom-modified carbon nitride polymers.

The effective generation and instant separation of photoexicited charge carriers are prerequisite for photocatalytic reactions, which can be analyzed by photoluminescence (PL) emission spectroscopy (Figure 5a), because photoluminescence stems from the recombination of free charge carriers. Relative to g-C_3N_4, the broad PL band at approximately 450 nm quenches quickly for P-CN, indicating that the recombination of electron−hole pairs occurring in the polymeric substrates is largely impeded. This is ascribed to the promoted electron relocalization on surface terminal sites after doping and structural advantages of P-CN, as the interconnected nanosheets can greatly curtail the diffusion distance of charge migration.[38,45] The low recombination rate is proposed to contribute to increase photoactivities and quantum yield. The transient photocurrent measurement was carried out to qualitatively investigate the separation efficiency of photoinduced charges during the photoreactions. It can be obviously seen that rapid and stable photocurrent responses are detected in both electrodes, and the photoresponsive phenomenon is entirely reversible upon each light excitation (Figure 5b). However, benefiting from more efficient light harvesting, the photocurrent for P-CN is much higher than that of pure bulky g-C_3N_4, revealing that the mobility of the charge carriers is efficaciously elevated.

EIS is a valid electrochemical approach to illustrate the electron-transfer efficiency at the electrodes. The semicircle in the EIS Nyquist plot in the middle frequency region is ascribed to the charge-transfer resistance R_{ct} along with the double-layer capacitance (CPE).[46,47] The Nyquist plot can be simulated well by an electrical equivalent-circuit model, wherein R_s represents the total Ohmic resistance of the electrolyte solution. In general, the smaller the diameter of semicircle arc of the EIS spectrum is, the lower the electron-transfer resistance value (R_{ct}) is, corresponding to more efficient separation and transport of photoexcited electron−hole pairs.[48−50] Figure 5c discloses similar semicircular Nyquist plots for both g-C_3N_4 and P-CN. However, P-CN features significantly smaller diameter, corresponding to a smaller contact and charge-transfer impedance. The larger semicircle radius for g-C_3N_4 can be due to the poorer electrical conductivity impeding the electron migration from carbon nitride to the back-contact electrode. In addition, the polarization curve of P-CN in the potential region of −1.5 to −0.9 V vs Ag/AgCl attributed to H_2 evolution[48,49] was measured with that of g-C_3N_4 as a control. As for P-CN, the much more pronounced cathodic current density and low overpotential indicate the boosted catalytic activity and reaction kinetics over g-C_3N_4 (Figure 5d), which is in accordance with the apparently improved photocatalytic hydrogen production rate detected on P-CN.

Both the PL spectra and electrochemical tests present the identical trend as the H_2 evolution performance, reflecting that generation, separation, and transfer efficiency of electrons in the g-C_3N_4 matrixes play a decisive role to influence the photocatalytic activity. Here, the P species in the carbon nitride framework can chemically bond with the C and N neighbors and force planar coordination, and the lone electron pair can delocalize to the π-conjugated tri-*s*-triazine of P-doped g-C_3N_4 that can serve as reinforcing active sites to some extent,[36] accordingly enhancing the conductivity and electron transfer capability. The thin nanosheets that constructed P-CN are quite propitious for photochemical reactions, beccause the

DOI: 10.1021/acsami.5b04947
ACS Appl. Mater. Interfaces 2015, 7, 16850−16856

reduced thickness can shorten charge transfer length from the bulk to the interface,[51−53] where the photoredox reaction takes places. Furthermore, the well-developed in-plane mesopores can also facilitate the charge and mass transport in the catalytic process.

4. CONCLUSIONS

A template-free methodology is presented to prepare mesoporous P-doped g-C_3N_4 nanostructured flowers through the condensation and thermolysis of melamine and orgaophosphonic acid. The low P concentration well retains the g-C_3N_4 polymeric framework, but the electronic properties have been seriously changed, causing not only red-shifted light absorption but also improved electronic conductivity. Additionally, the textual and structural features of high surface area associated with well-structured mesoporosity and nanosheet construction units ensure the excellent photocatalytic water reduction performance under visible light irradiation. It is anticipated that this simple but novel doping approach can be extended to prepare other chemically modified graphitic carbon nitride nanostructures, which hold great potential in various fields, such as photovoltaics, organic photosynthesis, electrocatalysis, and environmental remediation.

■ ASSOCIATED CONTENT

Supporting Information

TG curves of HEDP, g-C_3N_4 and P-CN, TEM images of P-CN and g-C_3N_4, N_2 adsorption−desorption curve and XPS spectrum of g-C_3N_4, comparison of FT-IR spectra and XRD pattern for P-CN before and after photocatalytic H_2 evolution, H_2 production performance versus P content in the doped graphitic carbon nitride. The Supporting Information is available free of charge on the ACS Publications website at DOI: 10.1021/acsami.5b04947.

■ AUTHOR INFORMATION

Corresponding Author

* E-mail: zyyuan@nankai.edu.cn.

Author Contributions

The manuscript was written through contributions of all authors. All authors have given approval to the final version of the manuscript.

Notes

The authors declare no competing financial interest.

■ ACKNOWLEDGMENTS

This work was supported by the National Natural Science Foundation of China (21421001), the Natural Science Foundation of Tianjin (15JCZDJC37100), the 111 project (B12015), and the Ph.D. Candidate Research Innovation Fund of Nankai University.

■ REFERENCES

(1) Kudo, A.; Miseki, Y. Heterogeneous Photocatalyst Materials for Water Splitting. *Chem. Soc. Rev.* **2009**, *38*, 253−278.
(2) Zhu, Y. P.; Ren, T. Z.; Ma, T. Y.; Yuan, Z. Y. Hierarchical Structures from Inorganic Nanocrystal Self-Assembly for Photoenergy Utilization. *Int. J. Photoenergy* **2014**, *2014*, 498540.
(3) Ran, J. R.; Zhang, J.; Yu, J. G.; Jaroniec, M.; Qiao, S. Z. Earth-Abundant Cocatalysts for Semiconductor-Based Photocatalytic Water Splitting. *Chem. Soc. Rev.* **2014**, *43*, 7787−7812.
(4) Zhu, Y. P.; Li, J.; Ma, T. Y.; Liu, Y. P.; Du, G. H.; Yuan, Z. Y. Sonochemistry-Assisted Synthesis and Optical Properties of Mesoporous ZnS Nanomaterials. *J. Mater. Chem. A* **2014**, *2*, 1093−1101.
(5) Zhu, Y. P.; Ma, T. Y.; Ren, T. Z.; Li, J.; Du, G. H.; Yuan, Z. Y. Highly Dispersed Photoactive Zinc Oxide Nanoparticles on Mesoporous Phosphonated Titania Hybrid. *Appl. Catal., B* **2014**, *156*, 44−52.
(6) Tada, H.; Fujishima, M.; Kobayashi, H.; Hisayoshi, K. Photodeposition of Metal Sulfide Quantum Dots on Titanium(IV) Dioxide and the Applications to Solar Energy Conversion. *Chem. Soc. Rev.* **2011**, *40*, 4232−4243.
(7) Samuel, T. D. W.; Turnbull, G. A. Organic Semiconductor Lasers. *Chem. Rev.* **2007**, *109*, 1272−1295.
(8) Forrest, S. R.; Thompson, M. E. Organic Electronics and Optoelectronics. *Chem. Rev.* **2007**, *109*, 923−925.
(9) Liu, J.; Liu, Y.; Liu, N.; Han, Y.; Zhang, X.; Huang, H.; Lifshitz, Y.; Lee, S. T.; Zhong, J.; Kang, Z. Metal-Free Efficient Photocatalyst for Stable Visible Water Splitting via a Two-Electron Pathway. *Science* **2015**, *347*, 970−974.
(10) Kuriki, R.; Sekizawa, K.; Ishitani, O.; Maeda, K. Visible-Light-Driven CO_2 Reduction with Carbon Nitride: Enhancing the Activity of Ruthenium Catalysts. *Angew. Chem., Int. Ed.* **2015**, *54*, 2406−2409.
(11) Zhu, Y. P.; Li, M.; Liu, Y. L.; Ren, T. Z.; Yuan, Z. Y. Carbon-Doped ZnO Hybridized Homogeneously with Graphitic Carbon Nitride Nanocomposites for Photocatalysis. *J. Phys. Chem. C* **2014**, *118*, 10963−10971.
(12) Chingin, K.; Perry, R. H.; Chambreau, S. D.; Vaghjiani, G. L.; Zare, R. N. Generation of Melamine Polymer Condensates upon Hypergolic Ignition of Dicyanamide Ionic Liquids. *Angew. Chem., Int. Ed.* **2011**, *50*, 8634−8637.
(13) Tian, J.; Liu, Q.; Asiri, A. M.; Alamry, K. A.; Sun, X. Ultrathin Graphitic C_3N_4 Nanosheets/Graphene Composites: Efficient Organic Electrocatalyst for Oxygen Evolution Reaction. *ChemSusChem* **2014**, *7*, 2125−2130.
(14) Dong, G.; Zhang, Y.; Pan, Q.; Qiu, J. A Fantastic Graphitic Carbon Nitride (g-C_3N_4) Material: Electronic Structure, Photocatalytic and Photoelectronic Properties. *J. Photochem. Photobiol., C* **2014**, *20*, 33−50.
(15) Cao, S.; Low, J.; Yu, J.; Jaroniec, M. Polymeric Photocatalysts Based on Graphitic Carbon Nitride. *Adv. Mater.* **2015**, *24*, 2150−2176.
(16) Zheng, Y.; Liu, J.; Liang, J.; Jaroniec, M.; Qiao, S. Z. Graphitic Carbon Nitride Materials: Controllable Synthesis and Applications in Fuel Cells and Photocatalysis. *Energy Environ. Sci.* **2012**, *5*, 6717−6731.
(17) Gong, Y.; Li, M.; Wang, Y. Carbon Nitride in Energy Conversion and Storage: Recent Advances and Future Prospects. *ChemSusChem* **2015**, *8*, 931−946.
(18) Niu, P.; Zhang, L.; Liu, G.; Cheng, H. M. Graphene-Like Carbon Nitride Nanosheets for Improved Photocatalytic Activities. *Adv. Funct. Mater.* **2012**, *22*, 4763−4770.
(19) Jun, Y. S.; Lee, E. Z.; Wang, X.; Hong, W. H.; Stucky, G. D.; Thomas, A. From Melamine-Cyanuric Acid Supramolecular Aggregates to Carbon Nitride Hollow Spheres. *Adv. Funct. Mater.* **2013**, *23*, 3661−3667.
(20) Sun, J.; Zhang, J.; Zhang, M.; Antonietti, M.; Fu, X.; Wang, X. Bioinspired Hollow Semiconductor Nanospheres as Photosynthetic Nanoparticles. *Nat. Commun.* **2012**, *3*, 1139.
(21) Zhang, J.; Zhang, M.; Yang, C.; Wang, X. Nanospherical Carbon Nitride Frameworks with Sharp Edges Accelerating Charge Collection and Separation at a Soft Photocatalytic Interface. *Adv. Mater.* **2014**, *26*, 4121−4126.
(22) Lee, E. Z.; Jun, Y. S.; Hong, W. H.; Thomas, A.; Jin, M. M. Cubic Mesoporous Graphitic Carbon(IV) Nitride: An All-in-One Chemosensor for Selective Optical Sensing of Metal Ions. *Angew. Chem., Int. Ed.* **2010**, *49*, 9706−9710.
(23) Liu, J.; Huang, J.; Zhou, H.; Antonietti, M. Uniform Graphitic Carbon Nitride Nanorod for Efficient Photocatalytic Hydrogen Evolution and Sustained Photoenzymatic Catalysis. *ACS Appl. Mater. Interfaces* **2014**, *6*, 8434−8440.

DOI: 10.1021/acsami.5b04947
ACS Appl. Mater. Interfaces 2015, 7, 16850−16856

(24) Tahir, M.; Cao, C.; Butt, F. K.; Idrees, F.; Mahmood, N.; Ali, Z.; Aslam, I.; Tanveer, M.; Rizwan, M.; Mahmood, T. Tubular Graphitic-C_3N_4: A Prospective Material for Energy Storage and Green Photocatalyst. *J. Mater. Chem. A* **2013**, *1*, 13949−13955.
(25) Tahir, M.; Cao, C.; Mahmood, N.; Butt, F. K.; Mahmood, A.; Idrees, F.; Hussain, S.; Tanveer, M.; Ali, Z.; Aslam, I. Multifunctional g-C_3N_4 Nanofibers: A Template-Free Fabrication and Enhanced Optical, Electrochemical, and Photocatalyst Properties. *ACS Appl. Mater. Interfaces* **2014**, *6*, 1258−1265.
(26) Gong, Y.; Li, M.; Li, H. R.; Wang, Y. Graphitic Carbon Nitride Polymers: Promising Catalysts or Catalyst Supports for Heterogeneous Oxidation and Hydrogenation. *Green Chem.* **2015**, *17*, 715−736.
(27) Zhao, Z.; Sun, Y.; Dong, F. Graphitic Carbon Nitride Based Nanocomposites: A Review. *Nanoscale* **2015**, *7*, 15−37.
(28) Yan, S. C.; Li, Z. S.; Zou, Z. G. Photodegradation of Rhodamine B and Methyl Orange over Boron-Doped g-C_3N_4 under Visible Light Irradiation. *Langmuir* **2010**, *26*, 3894−3901.
(29) Liu, G.; Niu, P.; Sun, C.; Smith, S. C.; Chen, Z.; Lu, G. Q.; Cheng, H. M. Unique Electronic Structure Induced High Photoreactivity of Sulfur-Doped Graphitic C_3N_4. *J. Am. Chem. Soc.* **2010**, *132*, 11642−11648.
(30) Zhang, Y.; Mori, T.; Ye, J.; Antonietti, M. Phosphorus-Doped Carbon Nitride Solid: Enhanced Electrical Conductivity and Photocurrent Generation. *J. Am. Chem. Soc.* **2010**, *132*, 6294−6295.
(31) Han, Q.; Hu, C.; Zhao, F.; Zhang, Z.; Chen, N.; Qu, L. One-Step Preparation of Iodine-Doped Graphitic Carbon Nitride Nanosheets as Efficient Photocatalysts for Visible Light Water Splitting. *J. Mater. Chem. A* **2015**, *3*, 4612−4619.
(32) Chen, S.; Qiao, S. Z. Hierarchically Porous Nitrogen-Doped Graphene−$NiCo_2O_4$ Hybrid Paper as an Advanced Electrocatalytic Water-Splitting Material. *ACS Nano* **2013**, *7*, 10190−10196.
(33) Chen, S.; Duan, J.; Tang, Y.; Qiao, S. Z. Hybrid Hydrogels of Porous Graphene and Nickel Hydroxide as Advanced Supercapacitor Materials. *Chem. - Eur. J.* **2013**, *19*, 7118−7124.
(34) Fang, Y.; Lv, Y.; Gong, F.; Wu, Z.; Li, X.; Zhu, H.; Zhou, L.; Yao, C.; Zhang, F.; Zheng, G.; Zhao, D. Interface Tension-Induced Synthesis of Monodispersed Mesoporous Carbon Hemispheres. *J. Am. Chem. Soc.* **2015**, *137*, 2808−2811.
(35) Zhu, Y. P.; Liu, Y. L.; Ren, T. Z.; Yuan, Z. Y. Hollow Manganese Phosphonate Microspheres with Hierarchical Porosity for Efficient Adsorption and Separation. *Nanoscale* **2014**, *6*, 6627−6636.
(36) Ma, T. Y.; Ran, J. R.; Dai, S.; Jaroniec, M.; Qiao, S. Z. Phosphorus-Doped Graphitic Carbon Nitrides Grown In Situ on Carbon-Fiber Paper: Flexible and Reversible Oxygen Electrodes. *Angew. Chem., Int. Ed.* **2015**, *54*, 4646−4650.
(37) Latorre-Sanchez, M.; Primo, A.; Garcia, H. P-Doped Graphene Obtained by Pyrolysis of Modified Alginate as a Photocatalyst for Hydrogen Generation from Water−Methanol Mixtures. *Angew. Chem., Int. Ed.* **2013**, *52*, 11813−11816.
(38) Lin, Z. Z.; Wang, X. C. Nanostructure Engineering and Doping of Conjugated Carbon Nitride Semiconductors for Hydrogen Photosynthesis. *Angew. Chem., Int. Ed.* **2013**, *52*, 1735−1738.
(39) He, F.; Chen, G.; Yu, Y.; Hao, S.; Zhou, Y.; Zheng, Y. Facile Approach to Synthesize g-PAN/g-C3N4 Composites with Enhanced Photocatalytic H_2 Evolution Activity. *ACS Appl. Mater. Interfaces* **2014**, *6*, 7171−7179.
(40) Xiang, Q.; Yu, J.; Jaroniec, M. Preparation and Enhanced Visible-Light Photocatalytic H_2-Production Activity of Graphene/C_3N_4 Composites. *J. Phys. Chem. C* **2011**, *115*, 7355−7363.
(41) Shi, L.; Liang, L.; Wang, F.; Ma, J.; Sun, J. Polycondensation of Guanidine Hydrochloride into A Graphitic carbon Nitride Semiconductor with A Large Surface Area as A Visible Light Photocatalyst. *Catal. Sci. Technol.* **2014**, *4*, 3235−3243.
(42) Gu, H.; Gu, Y.; Li, Z.; Ying, Y.; Qian, Y. Low-Temperature Route to Nanoscale P_3N_5 Hollow Spheres. *J. Mater. Res.* **2003**, *18*, 2359−2363.
(43) Mitoraj, D.; Kisch, H. On the Mechanism of Urea-Induced Titania Modification. *Chem. - Eur. J.* **2010**, *16*, 261−269.
(44) Choi, C. H.; Park, S. H.; Woo, S. I. Phosphorus−Nitrogen Dual Doped Carbon as An Effective Catalyst for Oxygen Reduction Reaction in Acidic Media: Effects of the Amount of P-Doping on the Physical and Electrochemical Properties of Carbon. *J. Mater. Chem.* **2012**, *22*, 12107−12115.
(45) Wang, X.; Maeda, K.; Chen, X.; Takanabe, K.; Domen, K.; Hou, Y.; Fu, X.; Antonietti, M. Polymer Semiconductors for Artificial Photosynthesis: Hydrogen Evolution by Mesoporous Graphitic Carbon Nitride with Visible Light. *J. Am. Chem. Soc.* **2009**, *131*, 1680−1681.
(46) Yang, W. H.; Wang, J. M.; Pan, T.; Xu, J. J.; Zhang, J. Q.; Cao, C. N. Studies on the Electrochemical Characteristics of $K_2Sr(FeO_4)_2$ electrode. *Electrochem. Commun.* **2002**, *4*, 710−715.
(47) Zhu, Y. P.; Ren, T. Z.; Liu, Y. P.; Yuan, Z. Y. In Situ Simutaneous Reduction-Doping Route for Synthesis of Hematite/N-Doped Graphene Nanohybrids with Excellent Photoactivity. *RSC Adv.* **2014**, *4*, 31754−31758.
(48) Ran, J. R.; Zhang, J.; Yu, J.; Qiao, S. Z. Enhanced Visible-Light Photocatalytic H_2 Production by $Zn_xCd_{1-x}S$ Modified with Earth-Abundant Nickel-Based Cocatalysts. *ChemSusChem* **2014**, *7*, 3426−3434.
(49) Hou, Y. D.; Laursen, A. B.; Zhang, J. S.; Zhang, G. G.; Zhu, Y. S.; Wang, X. C.; Dahl, S.; Chorkendorff, I. Layered Nanojunctions for Hydrogen-Evolution Catalysis. *Angew. Chem., Int. Ed.* **2013**, *52*, 3621−3625.
(50) Li, Q.; Meng, H.; Yu, J. G.; Xiao, W.; Zheng, Y. Q.; Wang, J. Enhanced Photocatalytic Hydrogen-Production Performance of Graphene−$Zn_xCd_{1-x}S$ Composites by Using an Organic S Source. *Chem. - Eur. J.* **2014**, *20*, 1176−1185.
(51) Ma, T. Y.; Dai, S.; Jaroniec, M.; Qiao, S. Z. Graphitic Carbon Nitride Nanosheet−Carbon Nanotube Three-Dimensional Porous Composites as High-Performance Oxygen Evolution Electrocatalysts. *Angew. Chem., Int. Ed.* **2014**, *53*, 7281−7285.
(52) Xie, G.; Zhang, K.; Guo, B.; Liu, Q.; Fang, L.; Gong, J. R. Graphene-Based Materials for Hydrogen Generation from Light-Driven Water Splitting. *Adv. Mater.* **2013**, *25*, 3820−3839.
(53) Xiang, Q.; Yu, J.; Jaroniec, M. Synergetic Effect of MoS_2 and Graphene as Cocatalysts for Enhanced Photocatalytic H_2 Production Activity of TiO_2 Nanoparticles. *J. Am. Chem. Soc.* **2012**, *134*, 6575−6578.

DOI: 10.1021/acsami.5b04947
ACS Appl. Mater. Interfaces 2015, 7, 16850−16856